HAL
open science

Fast-flame limit for hydrogen/methane-air mixtures

G. Ciccarelli, Nabiha Chaumeix, A.Z. Mendiburu, K. N'Guessan, A. Comandini

To cite this version:

G. Ciccarelli, Nabiha Chaumeix, A.Z. Mendiburu, K. N'Guessan, A. Comandini. Fast-flame limit for hydrogen/methane-air mixtures. Proceedings of the Combustion Institute, 2019, 37 (3), pp.3661-3668. 10.1016/j.proci.2018.06.045 . hal-02354698

HAL Id: hal-02354698

https://hal.science/hal-02354698

Submitted on 8 Feb 2022

HAL is a multi-disciplinary open access archive for the deposit and dissemination of scientific research documents, whether they are published or not. The documents may come from teaching and research institutions in France or abroad, or from public or private research centers.

L'archive ouverte pluridisciplinaire **HAL**, est destinée au dépôt et à la diffusion de documents scientifiques de niveau recherche, publiés ou non, émanant des établissements d'enseignement et de recherche français ou étrangers, des laboratoires publics ou privés.

Fast-flame limit for hydrogen/methane-air mixtures

G. Ciccarelli[a,*], N. Chaumeix[b], A. Z. Mendiburu[c], K. N'Guessan[b], A. Comandini[b]

[a]Queen's University, Canada

[b]ICARE CNRS-INSIS, France

[c]São Paulo State University, Brasil

*Corresponding Author:
Gaby Ciccarelli
Queen's University
Phone: +1 613 533-2586
Email: gaby.ciccarelli@queensu.ca

Colloquium : DETONATIONS, EXPLOSIONS, AND SUPERSONIC COMBUSTION including flame acceleration, DDT, and pulse- detonation, constant volume combustion, and scramjet-engines

Published in the 37th International Symposium on Combustion Proceedings

https://doi.org/10.1016/j.proci.2018.06.045

Fast-flame limit for hydrogen/methane-air mixtures

G. Ciccarelli[a], N. Chaumeix[b], A. Z. Mendiburu[c], K. N'Guessan[b], A. Comandini[b]

[a]Queen's University, [b]CNRS Orleans, [c]São Paulo State University

Abstract

Flame acceleration experiments were performed in a 10 cm inner-diameter tube filled with evenly spaced 0.43 blockage ratio orifice plates. The critical mixture composition required for flame acceleration to a fast-flame was measured for four methane/hydrogen fuel-air mixtures at initial temperatures of 298K, 423K, and 573K. These conditions provide a large range in the Zeldovich number between 12 and 28, where the Zeldovich number was calculated from the laminar burning velocity obtained from 1-D flame simulations. The data collapsed very well when the expansion ratio across the flame (calculated at the critical condition) was plotted versus the Zeldovich number. This is consistent with correlation proposed by Dorofeev [7], that was based on experimental data obtained over a narrower Zeldovich number range. For pure hydrogen fuel, the critical expansion ratio was found to be between 2 and 4, and for pure methane the critical expansion ratio was as high as 8, for an initial temperature of 573K.

Keywords: Fast Flames, Acceleration Criterion, Hydrogen, Methane

1. Introduction

The risk of an industrial plant explosion during the accidental release of a gaseous fuel depends on several factors, including the availability of an ignition source and the presence of an obstacle-congested

environment to promote flame acceleration. In most accident scenarios, it is difficult to predict the likelihood of ignition, and as a result, the conservative approach is to assume ignition. However, even if ignition is assumed, it does not necessarily guarantee that a dangerous overpressure will be generated. To obtain an overpressure in a vented industrial containment, such as a turbine exhaust duct, flame acceleration is required, and for fuel-air mixtures this requires obstructions in the flame path. There are many types of flame acceleration promoting obstacles that can be present in an industrial environment, including cross-flow oriented tubes, catwalks, conduit, wiring, pieces of equipment, etc. Therefore, every scenario presents a unique geometry and scale. To determine if flame acceleration could occur, large-scale experiments would have to be performed in the applicable geometry, and under prototypic thermodynamic conditions, that could include elevated pressure and temperature. This approach is rarely taken for economic and practical reasons; and in many cases, the ignition point is not known, so the results are not definitive. A more practical approach is to use laboratory-scale experiments to come up with a fundamental flame acceleration critical condition that does not depend on the channel scale or geometry.

Generally, in a geometry with lateral confinement, flame acceleration is driven by the expansion of the combustion products that induces a flow in the unburned gas ahead of the flame. Many experimental studies have been carried out in ducts with, and without obstacles, looking at flame acceleration. In smooth inner-surface tubes, the zero-velocity boundary condition produces a parabolic axial flow velocity profile across the diameter that results in stretching of the flame. The resulting increase in the flame surface area results in an increase in the volumetric burning rate that increases the flow velocity of the unburned gas ahead of the flame. This feedback loop, in conjunction with wall shear generated fine-scale turbulence, and thermal-diffusive flame surface instabilities leads to a prolonged flame acceleration [1]. As the flame accelerates to a velocity above the unburned gas speed of sound compression waves form that raise the temperature of the unburned gas ahead of the flame resulting in an increase in the laminar burning rate that further promotes flame acceleration. In unobstructed small diameter tubes, flame acceleration occurs

over a broad range of fuel-oxygen equivalence ratios that lead to deflagration-to-detonation-transition (DDT) [2, 3]. For fuel-air mixtures, more typical of industrial applications, only the most reactive mixtures, such as stoichiometric acetylene-air and hydrogen-air, produce flame acceleration to DDT in extremely long small-diameter tubes [4].

Shchelkin demonstrated that flame acceleration can be enhanced by roughening the tube wall by introducing a spiral wire into the tube [5]. This reduced dramatically the flame acceleration distance required for DDT. In the 1980s, experiments were carried out for a range of fuel-air mixtures in larger diameter tubes with repeated orifice plates [6]. The orifice plates, typically spaced at the tube diameter, introduce large perturbations to the unburned gas flow ahead of the flame that distort the flame, thereby increasing the flame area. The study revealed that flame acceleration could lead to two steady-state propagation regimes that were associated with significant overpressure generation at the front, i.e., fast-flames and quasi-detonations. For conditions that did not produce a fast-flame (e.g. slow-flame), the tube pressure rose uniformly but very little dynamic pressure at the flame front was observed.

Based on experimental data, Dorofeev proposed that the limit between the slow-flame and the fast-flame depends on the density ratio across the flame, $\sigma = \rho_u/\rho_b$, where the critical (or minimum) density ratio is given by σ^* [7]. He showed that for hydrogen and hydrocarbon fuels that σ^*depends on the Zeldovich number (β), which is given by $\beta = E_a*(T_b-T_u)/(R*T_b^2)$, where E_a is the activation energy, R is the gas constant, T_u is the initial mixture temperature and T_b the adiabatic flame temperature. Kuznetsov et al. [8] showed that there is no scale effect on this limit if the experiments are done in a setup where the turbulent length-scale is at least 100 times the flame thickness, which is the case in the 10 cm diameter tube used in this study.

The objective of this study is to measure the fast-flame limit in an orifice plate filled tube for H_2/CH_4-air mixtures. Hydrogen and methane were chosen because of the large difference in E_a, as well as the fact

that they are the main constituents of coke and syngas. The proportion of hydrogen and methane, along with initial temperature, were varied to get a wide spectrum in the Zeldovich number in order to develop a correlation as suggested in [7].

2. Experimental

The experiments were carried out in a 6.1 m long, 10 cm inner-diameter heated stainless steel tube shown in Fig. 1. The tube is covered in custom ceramic bead thermal blankets providing a temperature uniformity of 25°C on the inner surface. The pipe-sections and flanges are controlled separately. The tube is filled with 7.6 cm diameter orifice plates spaced at one-tube diameter. A capacitive discharge circuit delivering 500 mJ of energy across two electrodes was used to ignite the flame at the closed end of the tube. The test mixture is produced in a heated mixing chamber by first evacuating the chamber and then adding the gas components based on the method of partial pressures. The mixing chamber is equipped with a stirrer that is operated for 20 minutes to ensure mixture homogeneity. The 1.27 cm diameter tube between the mixing chamber and the test vessel is also heated to ensure that the mixture enters the tube at an elevated temperature. Six ionization probes (IP) are positioned along the tube, as per Fig. 1, to measure the flame time-of-arrival. The flame velocity is deduced based on the time-of-arrival between adjacent ionization probes. A PCB piezoelectric pressure transducer was used to measure the peak dynamic pressure. An amplified photodiode (PD) is located near the end of the tube to detect the light emitted from the flame. Experiments were carried out at an initial pressure of 101 kPa and at three initial temperatures (298K, 423K and 573K) with the following fuels: 100%H_2, 40%H_2/60%CH_4, 60%H_2/40%CH_4, 100%CH_4. The limit was obtained by varying the equivalence ratio, (which has a very small effect on the Zeldovich number) with the temperature and fuel composition held constant.

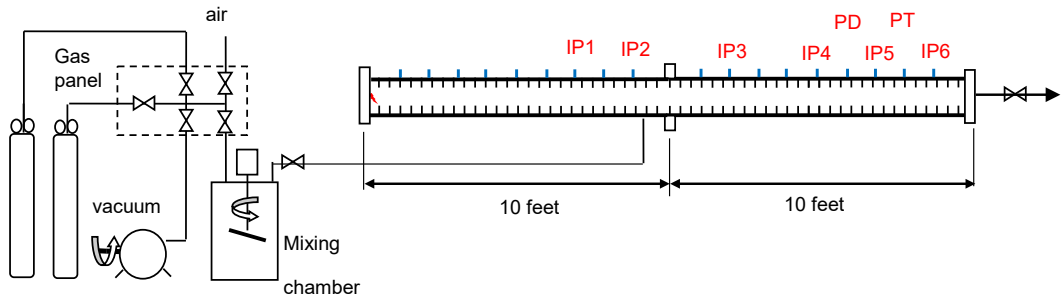

Fig. 1. Experimental flame acceleration setup showing ion probe positions.

The laminar flame speed was measured in a 56 L spherical bomb that has been previously described [9]. The 48 cm inner-diameter (56-litre) heated spherical stainless steel vessel is equipped with 4 quartz windows (100 mm optical diameter, 50 mm thickness). Thermal insulation applied on the outside of the bomb ensures a homogeneous temperature throughout the entire apparatus, to within ±1 K. The maximum test temperature was 473K. Two tungsten electrodes, located along the diameter of the sphere, was used to ignite the mixture. The gases were introduced directly in the spherical bomb using the partial pressure method. The pressures were measured using capacitive manometers (MKS Baratron, Type 631) to an accuracy of 0.5%. Experiments were carried out at an initial pressure of 101 kPa. Schlieren photography was used to visualize the spherical flame. A Phantom v1610 was used to capture the flame propagation at a rate of 19004 or 25000 frames per second, depending on the flame propagation speed range.

3. Results

First, the critical equivalence ratio (EQR), corresponding to the fast-flame limit, is reported from the flame acceleration experiments. The corresponding critical expansion ratio σ* is obtained using an equilibrium code. Then, this measured σ* is compared with the predicted critical expansion ratio using eqn. (1) where the Zeldovich number is obtained using the E_a obtained from a kinetics mechanism validated using the measured laminar burning velocity data over the initial temperature range of 298K - 473K initial temperature (but not for 573K).

3.1 Measured fast-flame limit

The flame velocity measurements down the tube, obtained from the six IPs, for 100%CH_4 and an EQR of 0.6 is provided in Fig. 2. The results from this mixture was chosen because it displays the different types of flame behaviour observed in these experiments. No flame was detected at 298K (i.e., no IP or PD signal detected), whereas, flame acceleration to a final velocity of 900 m/s (indicative of a fast-flame) was obtained at 573K. At the intermediate temperature of 423K, the flame initially accelerated to 182 m/s but then decelerated with no signals from the last two IPs. No PD signal was picked up either for the 423K test, so it can be concluded that the flame quenched before reaching the PD position (see Fig. 1)

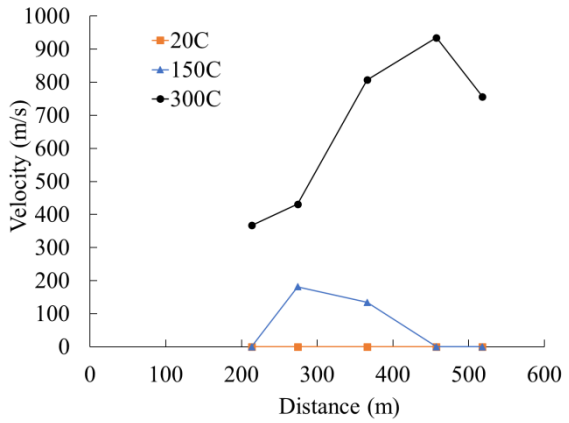

Fig. 2. Flame velocity versus distance for 100% and EQR=0.6 CH4 at three initial temperatures

A summary of the 100%CH_4 tests performed at 298K is provided in Fig. 3. For each test the average velocity measured in the first half of the tube (from ignition to IP2) and the second half of the tube (between IP3 and IP6) is shown in Fig. 3a. The peak pressure recorded is provided in Fig. 3b (note, the pressure profile for slow flames often show two peaks, e.g., Fig. 5b). Also shown in Fig. 3b (via the arrow on the x-axis) is the lowest EQR for which a PD signal was obtained. The results at EQR=0.65 produced no IP or PD signal. No pressure rise was recorded, so one can deduce either no ignition, or very early flame quenching. Two sets of data points are shown for an EQR of 0.68. In one test, the flame continuously accelerated to the end of the tube achieving a velocity of 600 m/s, typical of a fast-flame. In the other test,

the flame acceleration resulted in a peak flame velocity of 250 m/s at the end of the tube. This velocity is typical of a slow-flame, which based on other results, would have decelerated if the tube were longer. Based on these results, the fast-flame limit lies between 0.65 and 0.68. In general, higher EQRs resulted in more rapid flame acceleration producing fast-flames propagating in the velocity range of 600 m/s. Once the flame becomes a fast-flame the velocity oscillates about a mean value of around 600 m/s, and therefore the average velocity measured in the second-half can be smaller than that in the first-half, e.g., the test done at EQR=0.73 show this.

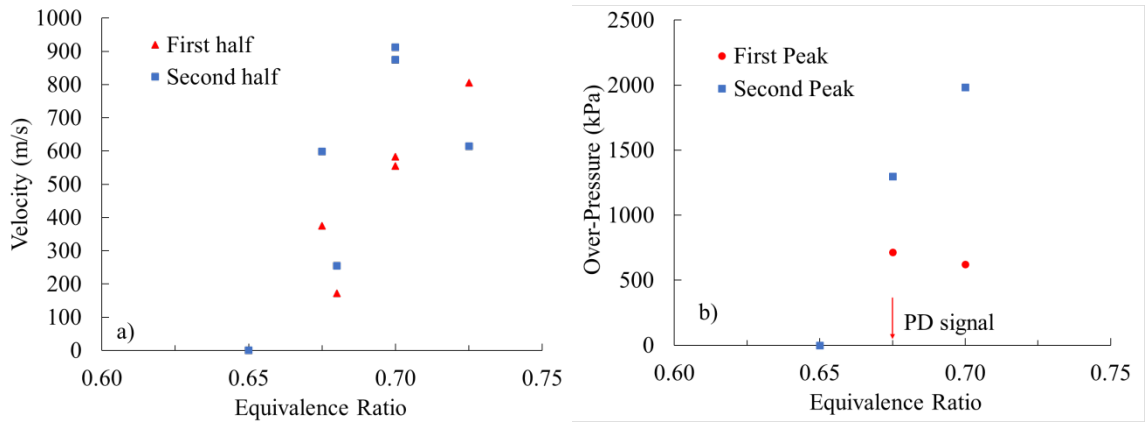

Fig. 3. Flame velocity (a) and peak pressure (b) measured for 100% methane at 298K

The results for 100%H_2 at 298K are provided in Fig. 4. The lowest EQR for which a flame was detected by the PD was 0.3, which resulted in a fast-flame. For the EQR=0.275 test, a small pressure rise was recorded but no flame was detected at the end of the tube by the PD, indicating that a flame was ignited but quenched before the PD. The small pressure rise was produced by the initial slow flame propagation that results in a uniform rise in pressure throughout the closed tube. The flame was too weak to be picked up by the IPs, or possibly quenched before the first ion probe. A test performed at EQR=0.3 resulted in flame acceleration to a velocity of just over 500 m/s, typical of a fast flame.

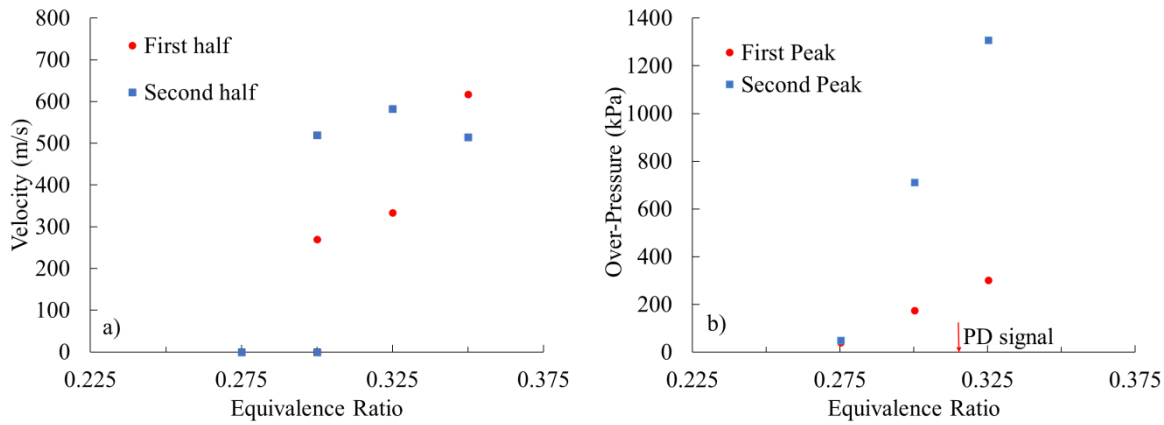

Fig. 4. Flame velocity (a) and peak pressure (b) measured for 100% hydrogen at 298K

Typical pressure traces obtained for tests producing a fast-flame and slow-flame are provided in Fig. 5a and 5b, respectively. One of the main differences in the pressure traces is the magnitude of the peak pressure. This can be attributed to the rate of combustion, as well as the energy release which is governed by the initial density of the mixture (double for the 298K compared to the 573K case). The fast-flame pressure trace is characterized by a rapid initial rise associated with a lead shock wave, whereas for the slow flame the pressure rises steadily to a peak value typical of uniform pressurization of a closed volume. If this was an open-ended tube, the same pressure trace would be obtained for the fast-flame, whereas the peak pressure for the slow-flame would be significantly lower than that recorded. Note, the oscillations observed in both traces, especially the fast-flame is produced by reflected shocks generated by the lead shock wave and the repeated obstacles. The large electrical noise in the slow flame pressure signal is due to the vertical-scale being very small because of the very low peak pressure recorded.

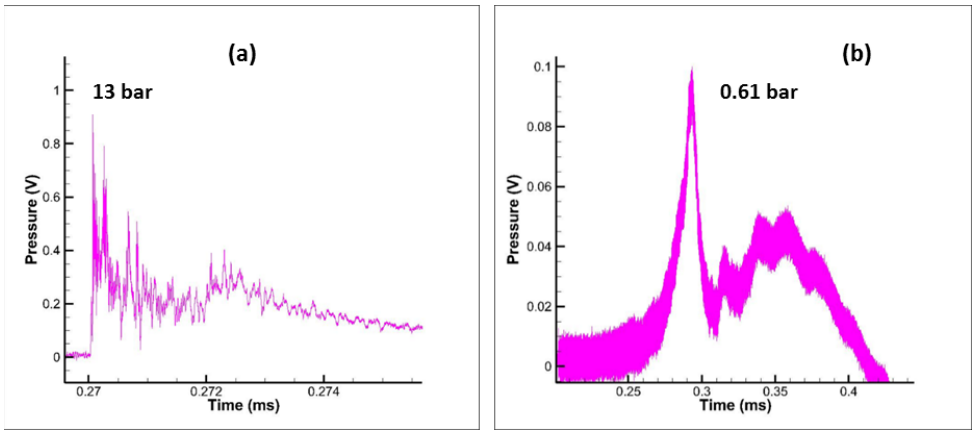

Fig. 5. Pressure trace obtained for 100% hydrogen, EQR=0.325 at an initial temperature of 298K (a) and 573K (b)

A summary of the fast-flame EQR limits for all four fuels, at the three different initial temperatures, are provided in Table 1. The fundamental driving force for flame acceleration is the product of the expansion ratio and the laminar burning velocity, both of which are affected by the initial temperature. As expected, the critical EQRs for hydrogen were significantly smaller than methane, presumably due to the significantly higher burning velocity of hydrogen. For the binary fuels, the critical EQR lies between the pure fuel values, proportionally to the amount of each constituent fuel. For the fuels containing methane, the critical EQR decreases, or remains the same, for increasing initial temperature. For hydrogen, there is a nonlinear effect of temperature on the critical EQR.

Table 1. Equivalence ratios corresponding to the measured fast-flame limits

	Initial temperature (K)		
Fuel	298	423	573
CH_4	0.675	0.63	0.55
$0.6CH_4 + 0.4H_2$	0.60	0.525	0.525
$0.4CH_4 + 0.6H_2$	0.525	0.45	0.45
H_2	0.30	0.25	0.35

3.2 Correlation of the fast-flame limit data

The fast-flame limit correlation requires the expansion ratio and the activation energy for the critical mixtures listed in Table 1. The expansion ratio was calculated using an equilibrium code. The activation

energy was obtained from the laminar burning velocity ($S_L°$) sensitivity to a small change in the adiabatic flame temperature (T_b). Specifically, the activation energy (normalized by the perfect gas constant) was obtained from the slope of the curve of $2*\ln(S_L°)$ versus $1/T_b$. The laminar burning velocity was calculated from the flame code COSILAB [11]. The GRI mechanism [12] was used for all the fuel mixtures, and cross referenced with the Mevel et al. mechanism [13], which has been validated for hydrogen fuel.

The applicability of the two mechanisms for such weak mixtures was not known. So spherical bomb tests, as described in the experimental section, were carried out to measure the laminar burning velocity to compare with numerical predictions using the two mechanisms. Note, the laminar burning velocity at 573K could not be obtained due to equipment limitations, instead values at the maximum test temperature of 473 are reported.

The flame morphology (smooth and spherical, wrinkled, smooth but with buoyancy effect) depends strongly on the composition and on the initial temperature. For the methane mixtures, the flames were spherical and smooth, and therefore it was straightforward to obtain a value for $S_L°$. For hydrogen, all the flames were wrinkled, and $S_L°$ was determined from the portion of the flame where, either the cells did not have time to fully develop, or developed only in a very limited fashion. For the hydrogen/methane mixtures, the flames were marginally ($60H_2/40CH_4$ at 473 K), or substantially (both binary mixtures at 298K and 423 K) affected. Figure 6 shows a series of flame images corresponding to each critical condition.

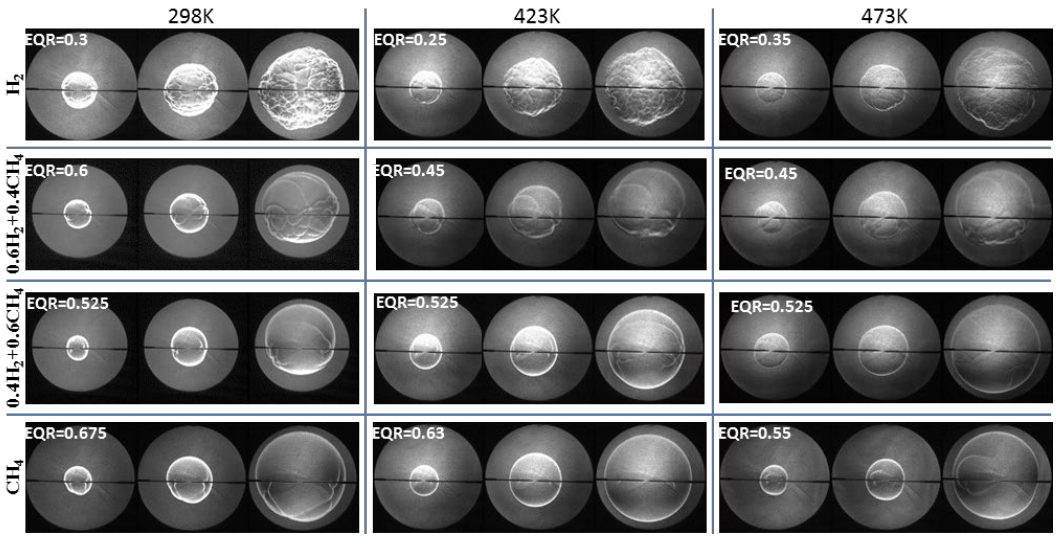

Fig. 6. Examples of flame images for the four studied fuels initially at 1 bar and different initial temperatures.

Depending on the morphology of the flame surface (smooth or wrinkled), two different in-house programs were used to obtain the temporal evolution of the flame radius from the schlieren images; from which the unstretched laminar flame speed of the unburned gases was derived. As described in [9, 10], the non-linear relationship between the flame speed and the stretch rate was used to derive the laminar burning velocity for each condition. Examples of the measured burning speed versus the stretch rate are provided in Fig. 7.

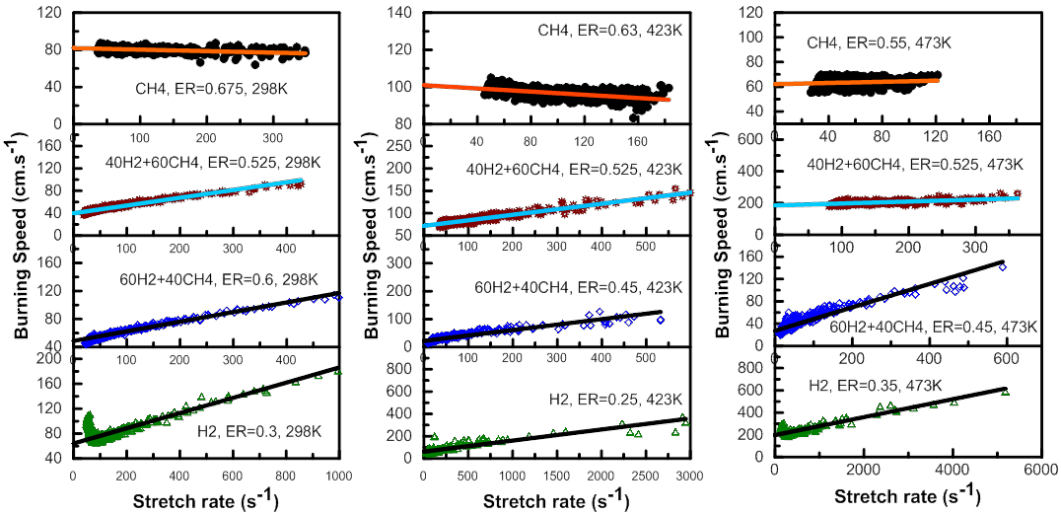

Fig. 7. Evolution of the burning speed with the stretch rate for the critical mixtures at 1 bar different initial temperatures.

The experimentally measured and simulated laminar burning velocities are summarized in Table 2. The agreement between the experimental measurement and that obtained using the GRI mechanism is very good for pure methane, but not so good for the other fuel mixtures. The discrepancy between the GRI and Mével mechanism for the pure hydrogen is only about 20%, giving some degree of confidence in the GRI mechanism even for the pure hydrogen fuel mixtures.

Table 2. Experimental and Simulated laminar flame speeds for the targeted mixtures.

fuel	T_i (K)	EQR	$S_L°$-Exp (cm/s)	$S_L°$-GRI (cm/s)	$S_L°$-Mével (cm/s)
CH_4	298	0.675	13.59	16.9	
CH_4	423	0.63	23.33	28.9	
CH_4	473	0.55	18.64	25.22	
$0.6CH_4+0.4H_2$	298	0.525	7.79	11.27	
$0.6CH_4+0.4H_2$	423	0.525	18.71	25.48	
$0.6CH_4+0.4H_2$	473	0.525	52.69	34.02	
$0.4CH_4+0.6H_2$	298	0.60	8.75	15.3	
$0.4CH_4+0.6H_2$	423	0.45	6.25	22.33	
$0.4CH_4+0.6H_2$	473	0.45	8.44	30.2	
H_2	298	0.3	17.08	6.62	7.74
H_2	423	0.25	23.36	10.45	12.36
H_2	473	0.35	68.60	38.53	47.85

For each of the critical mixtures (see Table 1), the adiabatic flame temperature (T_b), the activation energy obtained using the GRI and Mevel mechanisms, and the expansion ratio are all provided in Table 3. The measured critical expansion ratio from Table 3 is plotted as a function of the Zeldovich number in Fig. 8. The data points clearly show the separation between the slow and fast-flame propagation zones. All the data from the methane containing fuel mixtures correlate very well, whereas, the hydrogen data shows some anomalies, especially the 573K data point that doesn't follow the general trend. As proposed in the Dorofeev analysis [7], the following fast-flame limit correlation is obtained based on the data from the present data:

$$\sigma^{*}=-0.00285\beta^{2}+0.3823\beta+-2.2078 \quad (1)$$

This correlation, plotted in Fig. 8, predicts fairly well the limit between the slow and fast-flames observed in this study. All the data points lie at, or slightly below, the correlation curve, except for one of the hydrogen-air mixtures that lies above the curve.

Table 3. Comparison of measured and predicted values of the critical expansion ratio.

		Measured flame acceleration σ			σ* from eqn (1) using simulated S_L^o (Mével mech)			σ* from eqn (1) using simulated S_L^o (GRI mech)		
Fuel	Ti (K)	EQR	σ	T_b (K)	$Ea_{,Mével}$ (kJ/mol)	$\beta_{Mével}$	$\sigma_{Mével}$*	$Ea_{,GRI}$ (kJ/mol)	β_{GRI}	σ_{GRI}*
	298	0.675	6.11	1791	NA	NA	NA	493	28	6.20
CH_4	423	0.63	4.28	1810	NA	NA	NA	406	21	4.48
	573	0.55	3.12	1786	NA	NA	NA	355	16	3.25
	298	0.6	5.66	1687	NA	NA	NA	420	25	5.52
$0.6CH_4$ + $0.4H_2$	423	0.525	3.84	1649	NA	NA	NA	336	18	3.81
	573	0.525	3.04	1767	NA	NA	NA	334	15	2.99
	298	0.525	5.210	1569	NA	NA	NA	372	23	5.12
$0.4CH_4$ + $0.6H_2$	423	0.45	3.52	1525	NA	NA	NA	296	17	3.43
	573	0.45	2.81	1648	NA	NA	NA	307	15	2.78
	298	0.3	3.81	1183	223	17	3.48	199	15	2.97
H_2	423	0.25	2.63	1170	181	12	1.93	173	11	1.76
	573	0.35	2.52	1545	379	19	3.91	365	18	3.72

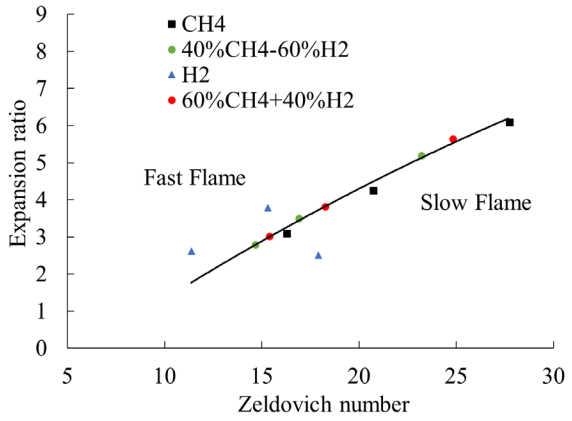

Fig. 8. Experimental fast-flame limit data along with the eqn. (1) correlation obtained using the GRI and Mével mechanisms.

4. Conclusions

Experiments were carried out to measure the fast-flame limits in a cylindrical tube equipped with orifice plates and to determine the fundamental combustion properties using spherical expanding flames coupled with detailed kinetic simulations. The tests were done over a broad range of Zeldovich numbers, obtained by varying the fuel composition of hydrogen/methane with air and the initial temperature. The data was well correlated when the flame expansion ratio was plotted versus the Zeldovich number, for each of the critical mixtures. A new correlation, based on the analysis of Dorofeev, was derived that predicts the measured fast-flame limit over this broad range of conditions (well within the +/-8% uncertainty quoted in [7]) except for the one data point obtained for pure hydrogen at 573K.

Acknowledgements

The first author is grateful for the financial support from Solar Turbines to perform the flame acceleration study under the guidance of Dr. Priyank Saxena. Dr. Mendiburu's stay at Queen's University was supported by FAPESP (Fundação de Amparo à Pesquisa do Estado de São Paulo) through Projects 2015/23351-9 and 2015/25435-5.

5. References

1. G. Ciccarelli, S. Dorofeev, Prog. Energy Combust. Sci. 34 (2008) 499–550.

2. P. Laffitte, P. Dumanois, Compt. Rend. Acad. Sci. Paris 100 (1926) 284.

3. A. Egerton, S. F. Gates, Proc. R. Soc. Lond. Ser. A 114 (1927) 152.

4. L. E. Bollinger. , AIAA Journal 2 (1) (1964) 131-133.

5. K.I. Shchelkin, J. Exp. Theor. Phys. 10, (1940) 823–827.

6. O. Peraldi, R. Knystautas and J.H. Lee, Proc. Combust. Inst. 21(1) (1986) 1629-1637.

7. S.B. Dorofeev, M.S. Kuznetsov, V.I. Alekseev, A.A. Efimenko, W. Breitung, J. Loss Prev. Process. Ind. 14 (2001) 583–589.

8. M.S. Kuznetsov, V I. Alekseev, A.V. Bezmelmtsyn, W Brettung, S.B. Dorofeev, I.D. Matsukov, A. Veser, and Y.G. Yankm, Report FZKA-6328, Karlsruhe Forschungszentrum Karlsruhe [Preprint IAE-6137/3, RRC Kurchatov Institute, Moscow] (1999).

9. J. Goulier, N. Chaumeix, F. Halter, N. Meynet, A. Bentaïb, Nuclear Engineering and Design 312 (2017) 14

10. D. Nativel, M. Pelucchi, A. Frassoldati, A. Comandini, A. Cuoci, E. Ranzi, N. Chaumeix, T. Faravelli, Combust. and Flame 166 (2016) 1-18

11. COSILAB, 2003-2017 by Rotexo GmbH & Co KG, http://www.rotexo.com

12. G.P. Smith, D.M. Golden, M. Frenklach, N.W. Moriarty, B.Eiteneer, M. Goldenberg, C.T. Bowman, R.K. Hanson, S.Song, W.C. Gardiner Jr., V.V. Lissianski, Z.Qin http://www.me.berkeley.edu/gri_mech/

13. R. Mével, F. Lafosse, N. Chaumeix, G. Dupré, C.E. Paillard, Int. J. Hydrog. Energy, 34 (21) (2009), 9007-9018

Fast-flame limit for hydrogen/methane-air mixtures

G. Ciccarelli[a,*], N. Chaumeix[b], A. Z. Mendiburu[c], K. N'Guessan[b], A. Comandini[b]

List of Figures caption

Fig. 1. Experimental flame acceleration setup showing ion probe positions.

Fig. 2. Flame velocity versus distance for 100% and EQR=0.6 CH4 at three initial temperatures

Fig. 3. Flame velocity and peak pressure measured for 100%CH4 at 298K;

Fig. 4. Flame velocity and peak pressure measured for 100%H2 at 298K.

Fig. 5. Pressure trace obtained for 100% hydrogen, EQR=0.325 at an initial temperature of 298K (a) and 573K (b)

Fig. 6. Examples of flame images for the four studied fuels initially at 1 bar and different initial temperatures.

Fig. 7. Evolution of the burning speed with the stretch rate for the critical mixtures at 1 bar different initial temperatures.

Fig. 8. Experimental fast-flame limit data along with the eqn. (1) correlation obtained using the GRI and Mével mechanisms.

List of Tables

Table 1. Equivalence ratios corresponding to the measured fast-flame limits

	Initial temperature (K)		
Fuel	298	423	573
CH_4	0.675	0.63	0.55
$0.6CH_4 + 0.4H_2$	0.60	0.525	0.525
$0.4CH_4 + 0.6H_2$	0.525	0.45	0.45
H_2	0.30	0.25	0.35

Table 2. Experimental and Simulated laminar flame speeds for the targeted mixtures.

fuel	T_i (K)	EQR	$S_L°$-Exp (cm/s)	$S_L°$-GRI (cm/s)	$S_L°$-Mével (cm/s)
CH_4	298	0.675	13.59	16.9	
CH_4	423	0.63	23.33	28.9	
CH_4	473	0.55	18.64	25.22	
$0.6CH_4+0.4H_2$	298	0.525	7.79	11.27	
$0.6CH_4+0.4H_2$	423	0.525	18.71	25.48	
$0.6CH_4+0.4H_2$	473	0.525	52.69	34.02	
$0.4CH_4+0.6H_2$	298	0.60	8.75	15.3	
$0.4CH_4+0.6H_2$	423	0.45	6.25	22.33	
$0.4CH_4+0.6H_2$	473	0.45	8.44	30.2	
H_2	298	0.3	17.08	6.62	7.74
H_2	423	0.25	23.36	10.45	12.36
H_2	473	0.35	68.60	38.53	47.85

Table 3. Comparison of measured and predicted values of the critical expansion ratio.

		Measured flame acceleration σ			σ* from eqn (1) using simulated S_L^o (Mével mech)			σ* from eqn (1) using simulated S_L^o (GRI mech)		
Fuel	Ti (K)	EQR	σ	T_b (K)	$Ea,_{Mével}$ (kJ/mol)	$\beta_{Mével}$	$\sigma_{Mével}$*	$Ea,_{GRI}$ (kJ/mol)	β_{GRI}	σ_{GRI}*
	298	0.675	6.11	1791	NA	NA	NA	493	33	6.89
CH_4	423	0.63	4.28	1810	NA	NA	NA	406	27	4.86
	573	0.55	3.12	1786	NA	NA	NA	355	24	3.71
	298	0.6	5.66	1687	NA	NA	NA	420	30	6.02
$0.6CH_4$ + $0.4H_2$	423	0.525	3.84	1649	NA	NA	NA	336	25	4.21
	573	0.525	3.04	1767	NA	NA	NA	334	23	3.49
	298	0.525	5.210	1569	NA	NA	NA	372	28	5.55
$0.4CH_4$ + $0.6H_2$	423	0.45	3.52	1525	NA	NA	NA	296	23	3.87
	573	0.45	2.81	1648	NA	NA	NA	307	22	3.31
	298	0.3	3.81	1183	223	17	3.90	199	20	3.47
H_2	423	0.25	2.63	1170	181	12	2.66	173	18	2.54
	573	0.35	2.52	1545	379	19	4.30	365	28	4.12